SF2A 2019
P. Di Matteo, O. Creevey, A. Crida, G. Kordopatis, J. Malzac, J.-B. Marquette, M. N'Diaye, O. Venot (eds)

MAGNETOSPHERIC ACCRETION IN THE INTERMEDIATE-MASS T TAURI STAR HQ TAU

K. Pouilly[1], J. Bouvier[1], E. Alecian[1], A.-M. Cody[2], J.-F. Donati[3], S.H.P. Alencar[4], K. Grankin[5], L. Rebull[6] and C. Folsom[3]

Abstract. Magnetospheric accretion is a main interaction process between Classical T Tauri stars (CTTSs) and their inner disk. Understanding this process is therefore crucial to characterize star-disk interactions. We investigate the photometric and spectroscopic variability of HQ Tau, a CTTS of 1.8 $M_\odot$ and 2.7 $R_\odot$, from Kepler K2 light curve and a series of ESPaDOnS spectra obtained at the Canada-France-Hawaii Telescope. Balmer line profiles exhibit periodic variability, at the stellar rotation period, with high velocity redshifted absorptions appearing (Inverse P Cygni Profile - IPC). The radial velocity shows a modulation at the stellar rotation period too, but is not consistent with the time of appearance of the IPC. We therefore ascribed the radial velocity modulation to a cold spot and the IPC to the accretion column. From the spectropolarimetric analysis of the ESPaDOnS spectra , we also measure a mean longitudinal magnetic field with a maximum intensity of 430 G, which is modulated by stellar rotation. The maximum is consistent with the IPC, we deduce that the mean longitudinal magnetic field is modulated by the hot spot thus corresponds to the footprint of the magnetic pole at the stellar surface. Preliminary results of this study appear to be consistent with what is expected from magnetospheric accretion onto a global dipolar magnetic field in the intermediate-mass T Tauri star HQ Tau.

Keywords: Classical T Tauri Star, IMTTS, HQ Tau, magnetospheric accretion, hot spot, cold spot

1 Introduction

Classical T Tauri Stars (CTTSs) are low or intermediate mass young stars. There are defined by their accretion disk and their magnetic field strong enough to truncate the disk near to the corotation radius and accrete material. The material follows the magnetic field lines to fall onto the star, forming the so called accretion columns. This complete process is the magnetospheric accretion process (Bouvier et al. 2007), and it is the key of evolution of young stellar objects. We present here the study of HQ Tau, an intermediate-mass CTTS, with the aim to characterize its magnetosphere and the interactions between the star and its disk. We use 2 data sets to lead this study: first the spectropolarimetry obtained from the ESPaDOnS spectrometer (Donati 2003) mounted at Canada-France-Hawaii Telescope (CFHT) between October 28^{th} and November 9^{th} 2017. This data set is composed of 14 spectra in the visible range at a resolution or 68 000 and a SNR of 150 at 730 nm. Then, the photometric study is performed thanks to the Kepler-K2 mission (`https://archive.stsci.edu/k2/`), which observed HQ Tau during the 13^{th} campaign. Section 2 presents the stellar parameters determination and modulation from both data sets. The spectroscopic study is detailed in Section 3 trough Hα and Hβ variability and we conclude this study by the spectropolarimetric analysis in Section 4.

[1] Univ. Grenoble Alpes, CNRS, IPAG, 38000 Grenoble, France
[2] Bay Area Environmental Research Institute, 625 2nd St Ste. 209, Petaluma, CA 94952
[3] Univ. de Toulouse, CNRS, IRAP, 14 avenue Belin, 31400 Toulouse, France
[4] Departamento de Fisica – ICEx – UFMG, Av. Antônio Carlos 6627, 30270-901 Belo Horizonte, MG, Brazil
[5] Crimean Astrophysical Observatory, Nauchny, Crimea 298409
[6] Infrared Science Archive (IRSA), IPAC, California Institute of Technology, 1200 E. California Blvd, MS 100-22, Pasadena, CA 91125 USA

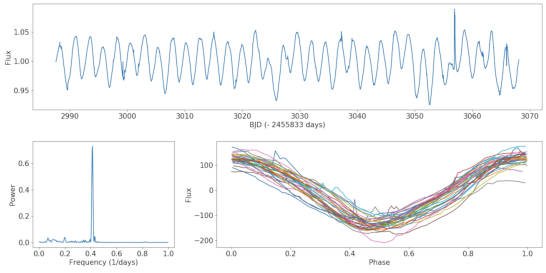

(a) **Top:** HQ Tau's Kepler K2 light curve. **Bottom left:** Lomb-Scargle periodogram with highest peak at 2.42 d. **Bottom right:** Light curve folded in phase.

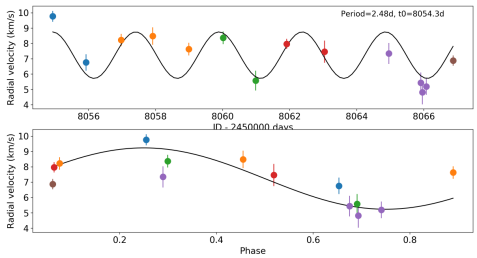

(b) **Top:** Radial velocity curve, each color correspond to a rotational cycle. **Bottom:** Curve folded in phase

Fig. 1

2 Stellar parameters

We take advantage of the high resolution spectra produced by ESPaDOnS to derive the stellar parameters of HQ Tau. First we fit a synthetic spectrum produced by the ZEEMAN code (Landstreet 1988; Wade et al. 2001; Folsom et al. 2012) on 11 wavelength windows of the mean spectrum to derive HQ Tau's T_{eff} = 4950 K and vsini = 53.7 km s^{-1}. Then we couple the effective temperature with the J and V magnitudes (Cutri et al. 2003; Norton et al. 2007), the Gaia parallax (Gaia Collaboration 2018), visual extinction (Herczeg & Hillenbrand 2014) and bolometric correction (Pecaut & Mamajek 2013) to derive the bolometric luminosity of the star. We fit its position in a Hertzprung-Russel Diagram with a CESTAM (Morel & Lebreton 2008; Marques et al. 2013) evolutionary model to derive the HQ Tau's mass M = 1.8 $M_{\odot}$ and radius R = 2.74 $R_{\odot}$. Finally, we derive a mean radial velocity v_{rad} = 7.14 km s^{-1}, by cross correlation on those wavelength windows with a photospheric template, Melotte 25 151, a K2 spectral type Main Sequence (MS) dwarf (Folsom et al. 2018).

As shown in Figure 1a, HQ Tau's light curve exhibits a clear and stable modulation. The periodogram analysis (Scargle 1982; Press et al. 1992) results clearly on a 2.42 d modulation, ascribed to the stellar rotational period as expected from a spotted surface (Herbst et al. 1994). A spot also induces a modulation of photospheric line profiles which produce an apparent modulation of the radial velocity (Vogt & Penrod 1983). We compute the radial velocity for each spectrum and plot the radial velocity curve shown in Figure 1b. A sinusoidal fit yields a period of 2.48 d, consistent with the photometric period. The curve folded in phase shows the behavior expected from a spot modulation. We set the phase at 0.5 at the moment when the spot is aligned with the line of sight.

3 Hα and Hβ profile

The most significant emission lines in HQ Tau's spectrum are Hα and Hβ. As there are in part formed in the accretion column, we can study them to get insight into the magnetospheric accretion process.

Figure 2 top panels shows the 14 profiles of those lines. We notice that there are very variable, especially in the red wings. Furthermore, using 2D periodograms presented in the bottom panels of Figure 2, Hα and Hβ exhibit a periodic modulation of this red wing, on the stellar rotational period. Those absorptions are Inverse P Cygni (IPC) profiles, produced by the accretion funnel flow, and are the direct signature of this phenomenon.

The 14 profiles are presented independently in Figure 3 sorted by days and by phase. This figure shows that the maximum of IPC profile is reach at phase 0.7, corresponding to the moment when the accretion funnel flow is aligned with the line of sight. This is not consistent with the radial velocity because the spot which modulates it is on the line of sight at phase 0.5. The two parameters are therefore modulated by two different phenomena, a cold spot for the radial velocity, and the funnel flow for the line profile.

We study the different components of those lines using the correlation matrices (Johns & Basri 1995; Oliveira et al. 2000; Alencar & Batalha 2002; Kurosawa et al. 2005) presented in Figure 4. Both Hα and Hβ line show a strong correlation within the red wing on there respective autocorrelation matrices and on the cross correlation matrix Hα vs. Hβ. On Hα autocorrelation matrix we notice also a correlation within the blue wing. Those correlations suggest that different physical processes dominate the variation of the blue and the red part of the

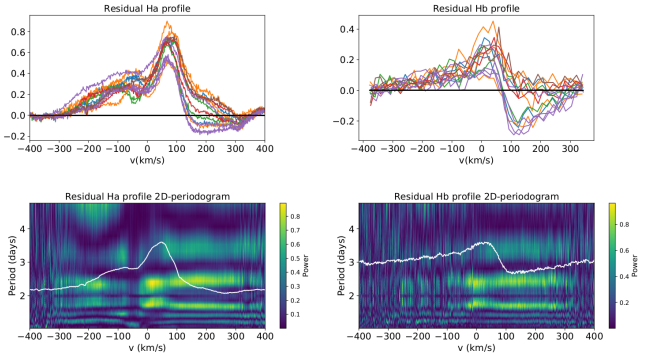

Fig. 2: **Top left:** 14 residual Hα profiles. **Bottom left:** 2D periodogram of Hα profile. **Right:** Same as left, but for Hβ profiles.

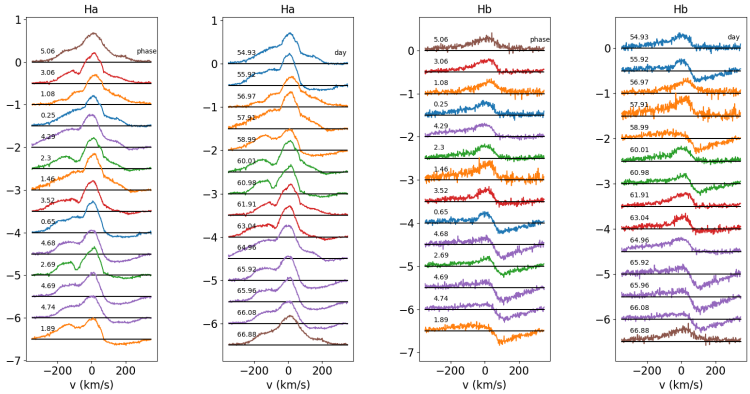

Fig. 3: **From left to right:** Successive Hα profiles sorted by phase, day, and the same for Hβ.

lines: accretion (IPC profile) for the red wing, and a wind for the blue wing of Hα. Finally, an anti correlation is highlighted on Hα (dark purple) between red and blue wing. This shows the possible accretion-ejection connection which will be detailed in a forthcoming paper (Pouilly et al., submitted).

4 Spectropolarimetry

Using the spectropolarimetric mode of ESPaDOnS, we get the unpolarized (Stokes I) and circularly polarized (Stokes V) spectra. We compute the Stokes I and V profiles by the Least Square Deconvolution (LSD - Donati et al. (1997)) method and study their variability. The Stokes I LSD profiles show a modulation which turns out to be periodic on the stellar rotational period. Unfortunately, only one third of the data set show a clear Stokes V signature, we are not able the derive any modulation from it. Nevertheless, we compute the surface average longitudinal magnetic field following the expression from Wade et al. (2001). The curve is shown in Figure 5. A sinusoidal fit yields to a period consistent with the photometric period. However the fit quality is low so the modulation is still unclear. The only correlation we can get from it is the consistency between the

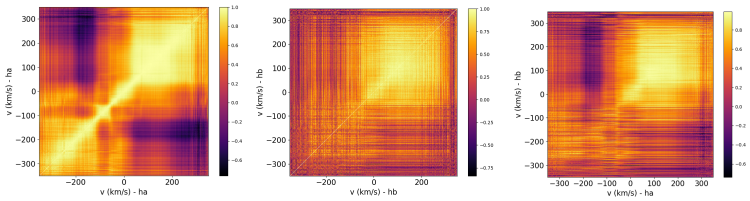

Fig. 4: **Left:** Hα autocorrelation matrix. **Middle:** Hβ autocorrelation matrix. **Right:** Hα vs. Hβ correlation matrix.

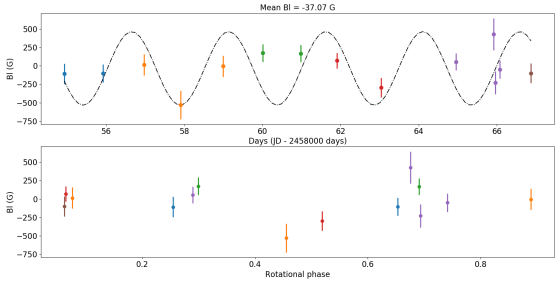

Fig. 5: **Top:** Surface averaged longitudinal magnetic field B_l curve. **Bottom:** B_l curve folded in phase.

strong minimum measured at phase 0.5, and the radial velocity curve, which indicates that the cold spot is on the line of sight at this phase.

5 Conclusions

The magnetospheric accretion process on HQ Tau is consistent with a strong magnetic field truncating the disk and the material being accreted along magnetic field lines. The accretion funnel flows are observed trough IPC profiles which modulate the Hα and Hβ lines while the radial velocity curve is modulated by a spot. From the estimated mass accretion rate, providing an estimate of the truncation radius, we conclude that the magnetospheric accretion process at work in low-mass T Tauri stars appears to extend to intermediate-mass ones.

This project has received funding from the European Research Council (ERC) under the European Union's Horizon 2020 research and innovation program (grant agreement No 742095 ; SPIDI : Star-Planets-Inner Disk- Interactions `spidi-eu.org`). This paper includes data collected by the Kepler mission. Funding for the Kepler mission is provided by the NASA Science Mission directorate. This work has made use of the VALD database, operated at Uppsala University, the Institute of Astronomy RAS in Moscow, and the University of Vienna. This project was funded in part by INSU/CNRS Programme National de Physique Stellaire and Observatoire de Grenoble Labex OSUG2020. Based on observations obtained at the Canada-France-Hawaii Telescope (CFHT) which is operated by the National Research Council of Canada, the Institut National des Sciences de l'Univers of the Centre National de la Recherche Scientifique of France, and the University of Hawaii.

References

Alencar, S. H. P. & Batalha, C. 2002, ApJ, 571, 378

Bouvier, J., Alencar, S. H. P., Harries, T. J., Johns-Krull, C. M., & Romanova, M. M. 2007, Protostars and Planets V, 479

Cutri, R. M., Skrutskie, M. F., van Dyk, S., et al. 2003, VizieR Online Data Catalog, 2246

Donati, J.-F. 2003, in Astronomical Society of the Pacific Conference Series, Vol. 307, Solar Polarization, ed. J. Trujillo-Bueno & J. Sanchez Almeida, 41

Donati, J.-F., Semel, M., Carter, B. D., Rees, D. E., & Collier Cameron, A. 1997, MNRAS, 291, 658

Folsom, C. P., Bagnulo, S., Wade, G. A., et al. 2012, MNRAS, 422, 2072

Folsom, C. P., Bouvier, J., Petit, P., et al. 2018, MNRAS, 474, 4956

Gaia Collaboration. 2018, VizieR Online Data Catalog, 1345

Herbst, W., Herbst, D. K., Grossman, E. J., & Weinstein, D. 1994, AJ, 108, 1906

Herczeg, G. J. & Hillenbrand, L. A. 2014, ApJ, 786, 97

Johns, C. M. & Basri, G. 1995, ApJ, 449, 341

Kurosawa, R., Harries, T. J., & Symington, N. H. 2005, MNRAS, 358, 671

Landstreet, J. D. 1988, The Astrophysical Journal, 326, 967

Marques, J. P., Goupil, M. J., Lebreton, Y., et al. 2013, A&A, 549, A74

Morel, P. & Lebreton, Y. 2008, Ap&SS, 316, 61

Norton, A. J., Wheatley, P. J., West, R. G., et al. 2007, A&A, 467, 785

Oliveira, J. M., Foing, B. H., van Loon, J. T., & Unruh, Y. C. 2000, A&A, 362, 615

Pecaut, M. J. & Mamajek, E. E. 2013, ApJS, 208, 9

Press, W. H., Teukolsky, S. A., Vetterling, W. T., & Flannery, B. P. 1992, Numerical recipes in FORTRAN. The art of scientific computing

Scargle, J. D. 1982, ApJ, 263, 835

Vogt, S. S. & Penrod, G. D. 1983, PASP, 95, 565

Wade, G. A., Bagnulo, S., Kochukhov, O., et al. 2001, A&A, 374, 265